IEEE Access
Multidisciplinary | Rapid Review | Open Access Journal

Received December 12, 2018, accepted January 10, 2019, date of publication January 23, 2019, date of current version February 14, 2019.

Digital Object Identifier 10.1109/ACCESS.2019.2894327

Design and Measurement of 3D Flexible Antenna Diversity for Ambient RF Energy Scavenging in Indoor Scenarios

DO HANH NGAN BUI[1], (Member, IEEE), TAN-PHU VUONG[1], (Senior Member, IEEE), JACQUES VERDIER[2], (Member, IEEE), BRUNO ALLARD[2], (Senior Member, IEEE), AND PHILIPPE BENECH[3], (Member, IEEE)

[1]IMEP–LAHC Laboratory, Grenoble INP, University of Grenoble Alpes, 38016 Grenoble, France
[2]Laboratory Ampère, Institut National des Sciences Appliquées de Lyon, University of Lyon, 69621 Villeurbanne, France
[3]G2Elab, Grenoble INP, University of Grenoble Alpes, CNRS, 38000 Grenoble, France

Corresponding author: Do Hanh Ngan Bui (do-hanh-ngan.bui@grenoble-inp.fr)

This work was supported in part by the ARC 4 Program of the Region Auvergne Rhône Alpes and in part by the FLAG-ERA JTC 2016 Convergence.

ABSTRACT Ambient radiofrequency (RF) energy scavenging has been recently addressed with a wide range of studies to provide alternative powering for low-power applications. However, due to the low power level of the ambient electromagnetic field, the efficiency of the latter systems is still below expectations. Multipath in the environment may be considered and antenna diversity is then a solution for quasi-omnidirectional RF reception to reach a higher probability of receiving energy in a realistic situation. A 3D flexible antenna diversity, which can be integrated into the rectangular packaging, is proposed in order to take advantage of system packaging form. The angle and polarization diversity antenna was designed on flexible substrate in order to achieve the flexibility and low-cost. This design overcomes the low performance of the substrate while maintaining a compact, high isolation, and good radiation efficiency of the antenna. An indoor experimental setup was carried out to compare different rectenna configurations. The measurement results validate the principle and demonstrate the performance of the 3D flexible diversity system. The probability measurements were carried out under precise conditions in indoor scenarios and the results in comparison with statistic models confirmed the performance of the system in such low power conditions.

INDEX TERMS Antenna diversity, indoor propagation, flexible structures.

I. INTRODUCTION

The wide availability of electromagnetic sources used in wireless communications nowadays is considered as a promising supply for ambient energy scavenging. A typical architecture for RF energy scavenging comprises a rectenna, i.e. an antenna and an RF-to-DC circuit (rectifier).

Numerous studies on rectenna design have been published, aiming for high efficiency with sufficient output power from very low input power [1]–[5] In a realistic environment, there is seldom a stationary position with a clear line-of-sight (LOS) between sources and scavenging systems. Further, indoor scenarios creates a multipath environment where signals may be reflected, diffracted or scattered. Therefore, the received power depends on environmental obstacles, as well as the source power and the distance. This creates a design challenge for energy scavenging antenna, requiring robust versatility to accommodate an unknown location, and unknown polarization of incident waves in case of a faded location.

To overcome these difficulties, mobile communication technologies integrate simultaneous multi-antenna from the multiple-input-multiple-output (MIMO) into a single design. However, this approach of multi-antenna in RF energy scavenging has not been broadly studied. Olgun *et al.* [1] presented a 3×3 planar antenna array connected directly to a 3×3 rectifier array in order to increase the harvested power and avoid complex feeds. As this design is planar, it can only capture energy in one direction. Kruesi *et al.* [6] have presented an idea of using six sides of a cubic structure in order to create a radiation pattern nearly isotropic. However, the design based on miniaturized dipole antenna with the maximum gain is 0.5 dBi, which is quite low in ambient

energy harvesting cases. In [2] the multi-direction harvested RF energy was demonstrated but only in two directions and no realistic measurement was conducted to verify the effectiveness of this principle. Zhang *et al.* [7], Zhong *et al.* [8] presented solutions of tri-band polarization-insensitive based on metamaterial but the demonstrators were not characterized with ambient density power, and the conversion of power to DC was not explored. This part is critical in low incident power environment. Some designs were validated by measurements in realistic indoor and outdoor environments, but any details of the direction setup and analysis of the design's influence on random locations were not presented [3], [4], [9]. Angle diversity antenna system was also presented as a prominent solution to step up the harvested energy [10], [11]. A multi-directional receiving system based on the association of 6 rectennas for home automation application, including in-situ measurements, was presented [11]. However, the circuit was designed on FR4 substrate; its shape occupied the volume of a cylinder, which has radius of 90 mm, and height of 54 mm. This design therefore not restrained by limited size or suitable material for Internet-of-things (IoT) applications.

With respect to the growing development of interconnected objects within the industry and domestic uses, the antenna in energy harvesting system must also meet a requirement for flexibility for its future integration within an object and the electronics for energy storage and conversion. In the context of wireless network sensors, a compact and flexible system is visibly required.

The system packaging of a conventional electronic circuit such as a rectangular box is considered here as a test vehicle. The antenna was adapted to the box features which can also be used for data transmissions. A flexible antenna substrate was used in order to achieve the low cost and facilitate mass production. As this type of substrate has the characteristic of high-loss and thinness; a compensatory technique is required to overcome this loss and maintain the gain of the antenna.

This paper proposes the design and characterization of a 3D flexible diversity antenna system in an office-like environment for energy harvesting from the Wi-Fi access point of Wireless Local Area Network (WLAN) sources, at the center frequency of 2.45 GHz [12]. The objective of this study is to confirm the performance of antenna diversity, under precise conditions with supportive results in comparison to statistical models [13] (next Section). The methodology used to achieve a high isolation across a multiple antenna system is presented in Section III. Measurements will focus on comparing probability density functions and cumulative density function of harvested power in different scenarios as in Section IV. The experimental results will be discussed in Section V.

II. DIVERSITY ANTENNA CONCEPT IN MULTIPATH ENVIRONMENT

In the domain of mobile communication, the multipath environment has been studied in order to determine algorithms to improve the performances of decoding processes. Various propagation models have then been proposed for both indoor and outdoor environments including large-scale path loss models and small-scale fading models [14].

The difference between indoor and outdoor environments is the layout of building structures, as well as the size and the materials of their walls, floors and other facilities. Multipath delays and the change in the envelope of the signal are characterized over a short travel distance, therefore the small-scale fading models were used to feature their propagation mode.

The distribution of the envelope of the received signal could be specified by different statistical model such as Ricean distribution, Rayleigh distribution, Suzuki model or Nakagami model [13], depending on the configuration between transmitters and receivers. These probabilistic models of received RF power have been demonstrated for realistic modeling of the multipath environment. The Ricean distribution was used while there is a dominant component such as the line-of-sight (LOS) propagation path. If this dominant signal was weaker or no dominant LOS signal detected, Rayleigh distribution was adapted. In case of multiple reflections and diffractions reached the receiver, the log-normal distribution is suitable for modeling the fading. The Nakagami distribution also can be used to model the dense scattering environment but in a more general approach and it can be deduced from one of aforementioned distributions.

It can be noticed that the WLAN sources are dynamic sources that use time-varying transmitted power and depend on the number of users on the network. Moreover, the power is not constant during transmission and depends on the types of protocols and modulations. Additionally, in typical office environments, there are often several Wi-Fi access points with the same characteristic of transmitter antenna, which operate at the same time, so interferences might also occur at the receiver location.

The probability of accessing the highest power source in a non-fixed location improves with the number of transmitters. However, this increase is non-linear due to the constructive and destructive combinations over space; varying amounts of received energy are expected at each receiver point [15]. Several studies are related to the propagation measurements in indoor multipath environments [16] and the obtained results for mean signal power levels were around 50 dB and 60 dB less than the signal power at the source. That means with a Wi-Fi source transmitting approximately 50 mW, the power level in the ambiance is estimated at about −34 dBm. This rather low power availability considerably reduces potential voltage at the rectifier circuit input and jeopardizes the overall efficiency.

Therefore, the antenna gain and radiation characteristics play an important role in the system's ability to amplify the signal level. The maximum directivity of antenna D_0 is calculated as follows [17]:

$$D_0 = \frac{4\pi}{\Omega_A} \tag{1}$$

where Ω_A represents the beam solid angle of antenna.

Observing (1), there is always a trade-off between the directivity aspect and the beam solid angle. Due to the unpredictable characteristic of the incident wave, isotropic or omnidirectional antenna are preferable to maximize potential power harvested.

The antenna must be directional to achieve the very high gain. A linear and planar antenna arrays are common solutions for this issue. The limitation here is that this usually has a higher gain and narrower beam solid angle, which is not the focus of this study.

The diversity antenna technique however is established as an effective solution to improve the performances of wireless service operating in a fading multipath environment. Diversity technique can be divided into different categories such as spatial diversity, polarization diversity and angle diversity. Spatial diversity respects the minimum distance between antennas as function of wavelength; polarization diversity makes use of different polarization of antennas and angle diversity combines different radiation patterns of different antennas in space.

For the applications based on rectangular shape of system packaging, the antennas are closely packed making spatial diversity too cumbersome to use.

This study proposes combining angle and polarization diversity metrics to take advantage of high gain and omnidirectional patterns at the same time. Multiple directional antennas are arranged in the environment space to maximize the chance of capturing ambient RF energy and increase the probability of harvesting energy above a certain level.

III. FLEXIBLE RECTENNA DESIGN

A. 3D ANTENNA DESIGN

The spatial output voltage distribution of the rectenna primarily depends on the radiation pattern of the antenna itself. Van Hoang *et al.* [18] have distributed a 3D voltage pattern measurement of a rectenna and then compared it with the 3D radiation pattern from the same antenna used in the rectenna.

Results showed both distributions having similar tendencies and the main lobe was situated in the same direction. For this reason, four antennas must be arranged in a way that their main lobes and beam solid angle could cover the maximum space, therefore increasing the spatial output voltage distribution.

In order to confirm the performance of angle diversity antenna in indoor scenarios, a first configuration is designed and analyzed by using the basic linear polarization microstrip patch antenna where the pattern maximum lobe is normal to the patch [17]. Four microstrip patch antennas were faced in opposite and perpendicular directions to take geometrical advantage of the packaging box (Fig. 1). Antenna elements were designed to operate at a frequency of 2.45 GHz, which is the central frequency of WLAN band. The substrate used for this design is Rogers 4003 with a thickness of 0.831 mm, a relative permittivity of 3.55 and a loss tangent of 0.0027. Antenna dimensions are 60 x 60 mm2 to reach the targeted

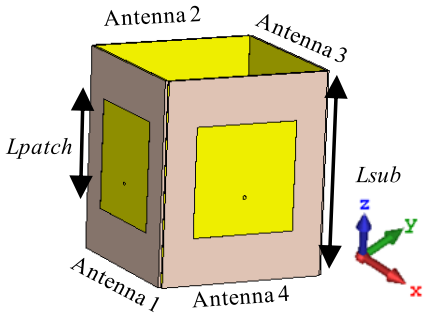

FIGURE 1. Structure of patch diversity antenna; Lpatch = 31.5 mm; Lsub=60 mm.

frequency band. Each antenna has a simulated gain near 5 dB and beam width of about 90°.

Due to the feeder position, the antennas have a vertical polarization with an E-field vector along the y-axis. The system thus has a quasi-omnidirectional pattern with maximum directivity in the four orthogonal directions.

In this configuration, the rectifier can be connected to four antennas inside the cube by SMA connector. Therefore, this structure cannot be simply adapted to the box features of a rectangular packaging as stated objective of the study. The mechanical assembly process seems to be easier by the involvement of flexible substrate.

However, this microstrip antenna technology cannot be applied to flexible substrates, which suffer of or from low performances, from high-losses or super thinness. Therefore, a novel design for flexible diversity antenna was proposed.

The design is based on the quasi-Yagi structure, which has the end-fire radiation characteristic. Four antennas are put together in order to have the same vertical polarization but different directions of propagation. The substrate used for this design is PET with a thickness of 0.175 mm, a relative permittivity of 3.21 and a loss tangent of 0.0049.

In order to form the diversity antenna by combining four antennas and arranging them around the rectangular form of the system packaging, the transmission line leading to each antenna has to be oriented in the same plane. One practical way to achieve this topology is to modify the feed line that has to be perpendicular to the end-fire radiation to avoid the conflict when connecting four antennas together.

In this case, we propose the structure with direct feed-line connection to the radiation arm as described in Fig. 2. This design allows easier integration between antennas and a common circuit. In this design, the driven element of the antenna operates like a monopole instead of a dipole as in the common design. Therefore, the length of the driven element is proportional with quarter-wavelength at the design frequency. The second arm of the driven element is thus not necessary. The directors still have the length proportional with half-wavelength in order to maintain the directivity of the antenna. The structure consists of a reflector, printed on the back of the substrate, which is connected with the common ground plane, in order to produce the end-fire radiation

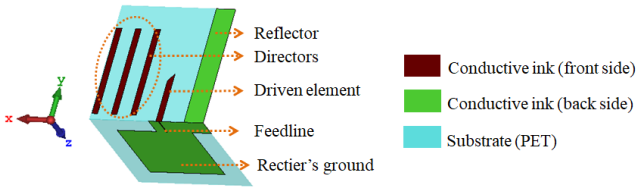

FIGURE 2. 3D structure of the proposed flexible antenna, taken into account the common ground of the rectifier.

pattern. The rectifier will be used to connect four antennas together, thus the design of one antenna has to take into account the influence of the rectifier's ground. The simulated reflection coefficient and radiation pattern of this antenna are presented respectively in Fig. 3(a) and (b). The antenna has a simulated radiation efficiency of 96.5% and simulated total efficiency of 96.4%.

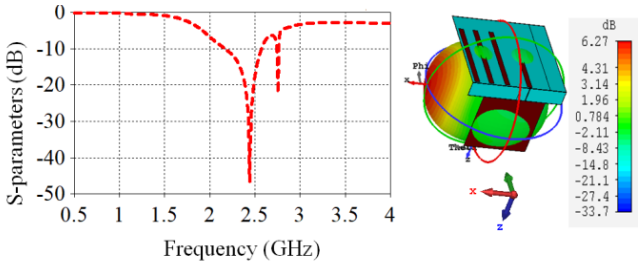

FIGURE 3. (a) Simulated reflection coefficient; (b) Radiation pattern of proposed antenna, gain of 6.27 dBi.

This same design is applied for each antenna on the four sides of the cube. The arrangement of four antennas into one antenna diversity system has a great significance on the radiation pattern of the system. The essential challenge of packed multi-antenna is to decrease the mutual coupling effects between antennas, which can affect the input impedance and radiation pattern of each element. If four antennas are arranged in the cascade topology, the radiation pattern of each antenna will be degraded notably because of the placement of the ground in the direction of propagation. Therefore, four antennas have been arranged in two pairs with a same ground and placed one pair opposite to the other (Fig. 4a).

Nevertheless, while placing four antennas together on top a system packaging, the mutual coupling appears, especially between the two pairs ANT1- ANT2 and ANT3- ANT4, as in these two pairs, the antennas are closer one to the other. The mutual coupling is only serious and noteworthy between two antennas that lie on propagation direction one of the other. The S-parameters are presented in Fig. 4b showing a mutual coupling of about 6 dB between these antennas and therefore degrading the total efficiency. The total efficiency of four antennas is lower down to 71% compared to 96.4% for only one antenna. The techniques to reduce mutual coupling between antennas is necessary to ensure the operation of the diversity antenna.

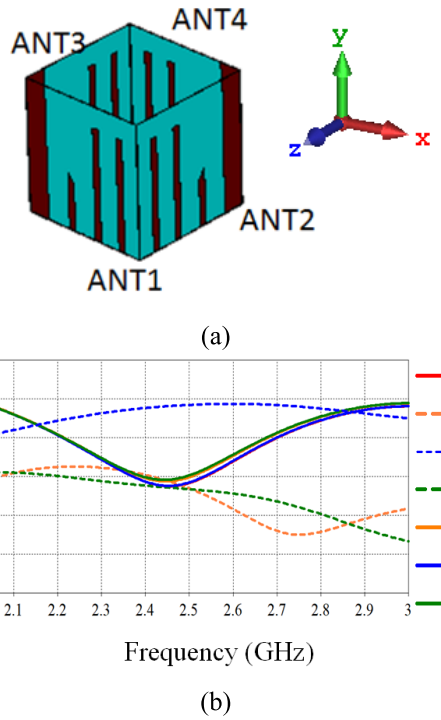

FIGURE 4. (a) Configuration of four antennas in the form of a system packaging; (b) S-parameters of four antennas.

The essential challenge of packed multi-antenna is to decrease the mutual coupling effects between antennas, which can affect the input impedance and radiation pattern of each element. Several decoupling methods for multiple antenna system were presented in literature, including defected ground structure (DGS) [19], [20], collocated orthogonal polarization, and decoupling networks, or parasitic elements [21].

In this design, all the antennas have the same vertical polarization. The structure of the driven and director element remains the same as the structure of one antenna, as described in Fig. 2. Hence, the technique for reducing mutual coupling is proposed by slightly changing the polarization of each antenna. The direction of the driven element along the director element is adjusted in order to not match the other ones' polarization as described in Fig. 5. The parameter *da* is a function of the angle α between the original position and inclined position; the longer the value *da*, the larger the angle α and the higher the isolation between ports. However, the directivity of each antenna has been affected and the optimization process has to take into account the total efficiency of the diversity.

The driven element then has been optimized to have the tilt of about 15^0 compared to the original direction. By changing this parameter, the decoupling frequency can be controlled and therefore the performances of the diversity antenna can be assured. It has to be noted that the spacing between ports of ANT1 to ANT2 (as ANT3 to ANT4) is about 0.5 λ_0 at original position and about 0.41 λ_0 at inclined position,

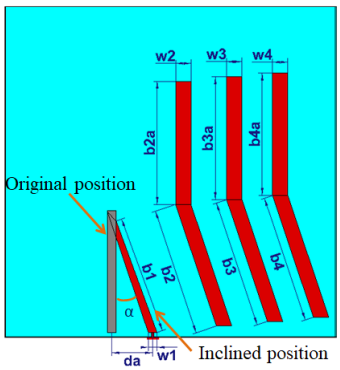

FIGURE 5. Details of inclined position of driven and director element; b1=23.3mm, b2=b3=b4=25.2 mm, b2a=24.3 mm, b3a=24.2 mm, b4a=24.1 mm, w1=1.7 mm, w2=w3=w4=3 mm, da=8 mm.

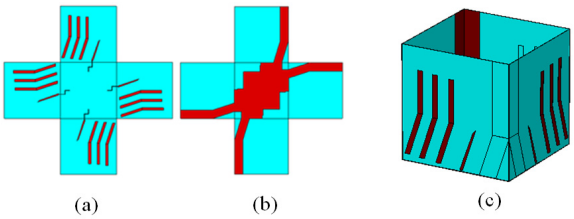

FIGURE 6. Configuration of the proposed diversity antenna (a) Flat structure, top view; (b) Flat structure, bottom view and (c) 3D Folded structure.

with $\lambda_0$is the wavelength in air. This remark suggests that the amount of mutual coupling in this configuration depends mainly on the relative orientation of each antenna and their radiation pattern instead of the relative separation between them. The final design is presented in Fig. 6a,b. The simulated mutual coupling between two antennas ANT1 and ANT2 is presented in Fig. 7. Applying the polarization changing technique, the mutual coupling between antennas is reduced from −6 dB to −33 dB at frequency 2.4 GHz.

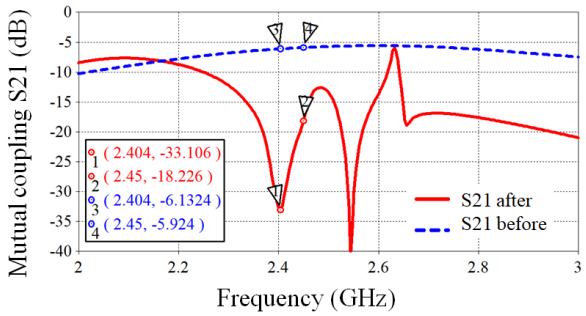

FIGURE 7. Mutual coupling between two antennas ANT1 and ANT2 before and after reducing the mutual coupling.

The overall system in the system packaging form is presented in Fig. 6c. Thanks to the flexible characteristic of the substrate, the rectenna has been bent from the flat structure to this 3D configuration without further support for connection between perpendicular planes. The optimized design has the size of 65 × 65 × 65 mm3. The calculated radiation efficiency is 91 % for the adjusted antenna compared to 71% without a decoupling technique. The antenna system has a simulated

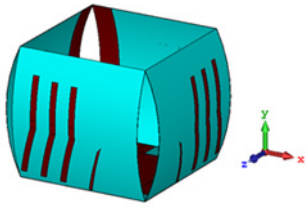

FIGURE 8. Deformed system by pressure from axis-y, Bending radius Rb= 70 mm.

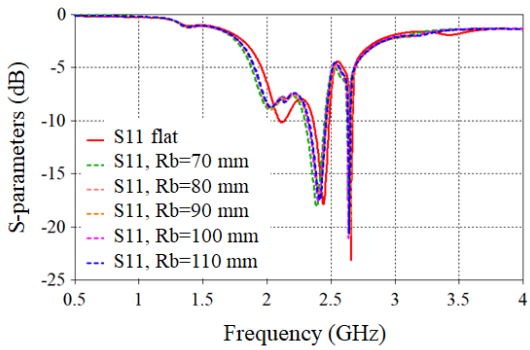

FIGURE 9. Simulated reflection coefficient of bending antennas at different bend radius *Rb* (mm).

gain of 6.2 dBi in each direction, in quasi-vertical polarization. Additionally, the polarization was extended from vertical to few degrees (about 15^0) and therefore it creates the polarization diversity of the system. This diversity brings out one important benefit for the system, in particular for mobile objects.

An analysis of antenna deformation was carried out to evaluate the performance of the system. It has to be noted that the substrate PET, thickness of 0.175mm is a stiff and dimensionally stable material. In this configuration of 3D-cube, each antenna is affixed with others by three edges. The form will be maintaining with the support of the packaging of the circuit. Therefore, it is not evident to be deformed easily. The magnitude of deformation is limited in this case. The antennas were bent with the bend radius *Rb* from 70 to 110 mm as described in Fig. 8. The system is not supposed to be bent deliberately with smaller radius than that in reality. The simulated S-parameters and realized gain of the analysis is presented in Fig. 9 and Fig. 10, respectively.

The reflection coefficient has been slightly changed, which indicates that the proposed antenna preserve its resonant frequencies. Regarding the radiation properties, the radiation pattern maintains its form and the gain is slightly changed due to the deformation of the antenna. The results suggest that the performance of the system is preserved under limited deformation, due to fixed configuration of the packaging form.

B. RECTIFIER STRUCTURE

The rectenna diversity is composed of four antennas and a circuit board whose inputs are microstrip lines. In this study,

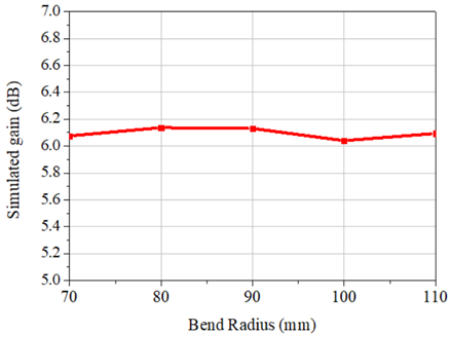

FIGURE 10. Simulated gain (dB) of bending antennas at different bend radius *Rb* (mm).

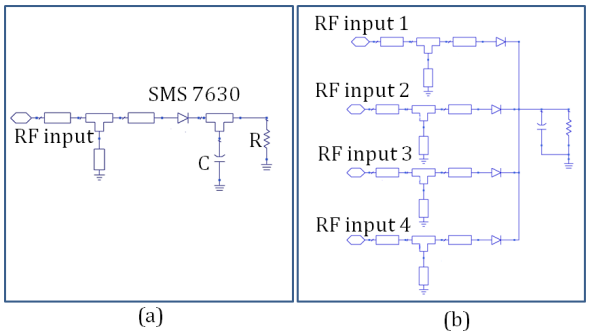

FIGURE 11. Structure of proposed rectifiers: (a) Schematic of single input rectifier (A); (b) Schematic of multi-input rectifier (B).

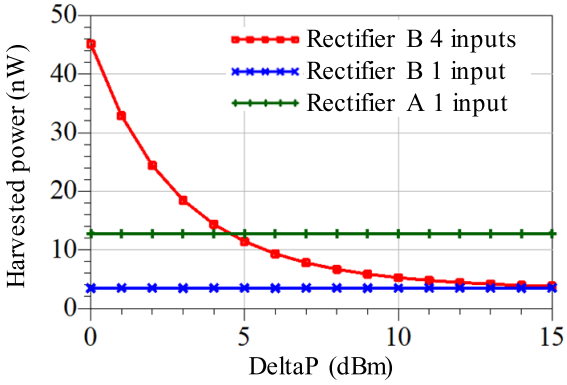

FIGURE 12. Simulated output power versus difference of levels (DeltaP) between branches of rectifiers A and B on Rogers 4003 substrate, at input power of −34 dBm.

we use the conventional 50-Ω impedance interface between antenna and rectifier to simplify design and tests.

The rectifier is a four-port circuit, which consists of four identical rectifiers; the harvested power is combined at the DC level.

The rectifier can be connected with the diversity of four patch antennas through a SMA connector. In cases of flexible diversity, the circuit can be directly implemented on the same flexible substrate of the antennas and therefore it is not necessary to build the transition part between antennas and rectifiers. However, due to the thinness of the PET flexible substrate, the conductor loss will be significantly large and can reduce the efficiency of the rectifier. As a result, using a separate circuit with another substrate (like Rogers 4003) could be one solution.

1) SEPARATE CIRCUIT DESIGN

Two rectifier designs were proposed, corresponding to various configurations of measurement (Fig. 11): rectifier A for a single antenna, on RO 4003 substrate; rectifier B for four antennas, on RO 4003 substrate. Rectifiers were designed using Agilent ADS software. The series single diode topology was chosen for low input power [22]. The circuits A and B have been implemented on Rogers RO 4003 substrate and have been optimized over the power input range of −45 dBm to −20 dBm. The rectifier device is a Schottky diode SMS7630. Rectifier A was designed to have a maximum power point at −35 dBm and the load of 5.6 kΩ, what is close to the junction parasitic resistance of the diode. It can be noted that the junction parasitic resistance of a Schottky diode can be deduced from the current-voltage (I-V) characteristics, given by Shockley diode equation. The parallel structure in [4] was selected to design rectifier B that combines the DC output of four rectifiers. A load of 1.8 kΩ was selected in order to maximize output power in case the rectifier only had one main source and other branches were not excited. Consequently, the efficiency of the rectifier in this case was degraded compared to Rectifier A, since each branch does not operate at its maximum power point, and the lower energy branches played as passive loads on the main branch. Fig. 12 shows the simulation of output power versus the disparity of input power between branches of rectifier B, in comparison with rectifier A and rectifier B with only one input. Parameter *DeltaP* represents the difference between highest input level and others of Rectifier B. Results show that with the difference between the highest branch and others as being less than 5 dB, this structure would deliver better output power compared to a single input rectifier.

For the connection between flexible antennas and Rectifier B, instead of using a board-to-board connector, which is expensive and not suitable to hold the flexible antenna, this study proposes to add a transition part between the antennas and the circuit. Each antenna has a transition part, which is folded of 90 degrees from the antenna plane and consists of two segments of the line. One segment is the feed line of the antenna and the other is the common line with the circuit.

The circuit is placed in coincidence with four transition parts and is connected to them by eight screw connectors (Fig. 13). The common transmission lines are then affixed together by silver solder. The holes created for screw connectors also have the role of alignment guide between circuits.

The impedance of transmission line of each segment is now decided by the effective permittivity formed by the combination of two substrates. The simulated insertion loss of the connection at 2.45 GHz is about 0.2 dB. This structure allows the low-loss connection between antennas and the rectifier circuits and therefore maximizes the harvested energy.

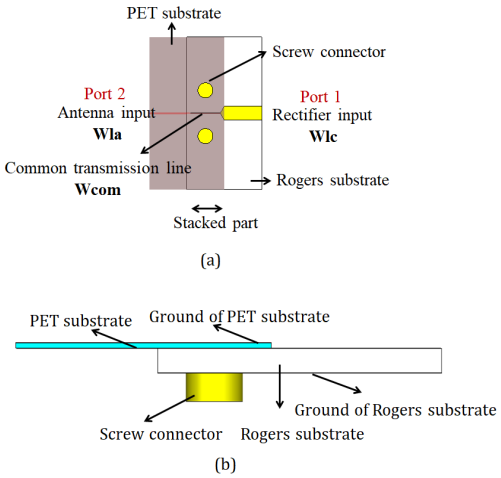

FIGURE 13. Transition part between one antenna and separated rectifier: (a) Top view Wla=0.4 mm, Wlc=1.7 mm, Wcom=0.3 mm; (b) Side view.

2) ON FLEXIBLE-SUBSTRATE RECTIFIER

The same principle of rectifier B was used to design the rectifier C on the same PET substrate as the antenna.

With lower permittivity, the guided wavelength in the circuit is longer and the circuit has a larger size as compared to the designed circuits on Rogers substrate. In order to fit into the reserved area of the designed antennas diversity, the miniaturization of the circuit is necessary and the meander design technique was applied. The matching circuit consists of an open circuit, better than a short-circuit, which will complicate the fabrication process. Fig. 14 describes the rectifier circuit in details and its implementation in the antenna diversity.

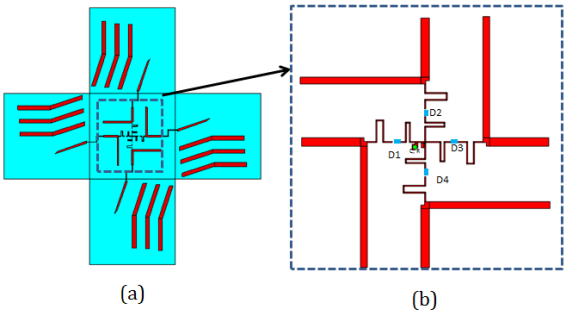

FIGURE 14. (a) On-flexible-substrate rectifier C with the antenna diversity; (b) Details of the rectifier circuit C.

The circuit is based on microstrip technology that has three loss mechanisms: conductor loss, dielectric loss and radiation loss. Due to the small thickness of 0.175 mm, the conductor loss will dominate and therefore increases the insertion loss of the circuit. The simulated results show that with the very thin substrate, the efficiency of the rectifier is actually degraded and therefore the harvested power will be lower than that from Rogers substrate-based circuits (Fig. 15). However, the advantage of this solution is in the easy fabrication process: the whole rectenna system can be printed in one step, at the same time limiting the insertion loss in transition parts between two substrates.

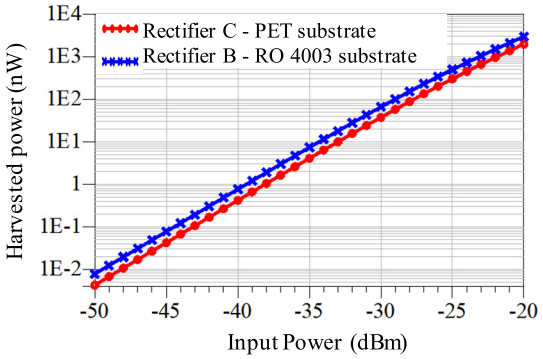

FIGURE 15. Simulated harvested power from rectifiers C using PET and rectifier B using RO 4003 substrate respectively, as function of input power with difference DeltaP between ports of 5 dB.

IV. EXPERIMENTAL SETUP

The first measurement was conducted to obtain the characteristics of a designed multi-antenna system. The return loss, isolation and radiation pattern measurements are realized using the vector network analyzer (VNA) in an anechoic chamber.

The second measurement to evaluate the performance of the rectennas is performed in various scenarios listed in Table 1, describing different configurations towards antenna combinations in a realistic environment. These configurations have been performed in 98 points in an office room of 4.2 m × 2.1 m. For each point, 11 separated measurements have been conducted corresponding to 5 scenarios and have given 1078 measurements in total.

TABLE 1. Measurement scenarios.

	Rectenna	Antenna	Rectifier	Points
S1		1 x Patch	-	4x98
S2	Rectenna 1A	1 x Patch	Rectifier A	4x98
S3	Rectenna 1B	4 x Patch	Rectifier B	98
S4	Rectenna 2	Proposed diversity	Rectifier B	98
S5	Rectenna 3	Proposed diversity	Rectifier C	98

The scenario S1 was conducted in order to estimate the available power in ambiance at each point and each direction, using a conventional antenna patch.

The scenario S2 used a conventional antenna patch and rectifier A (Rectenna 1A) (Fig.17a) to measure the harvested power at each point and each direction.

The scenario S3 used 4 patch antennas in opposite and perpendicular directions to take geometrical advantage of the packaging box, associated with Rectifier B (Rectenna 1B - Fig.17b). It is a scenario that aims to evaluate

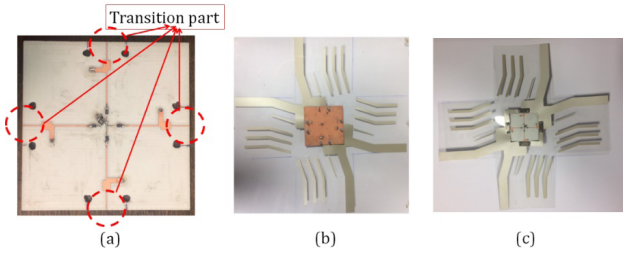

FIGURE 16. The separated rectifier: (a) fabricated 4-port rectifiers with transition part; (b) connected diversity rectenna (bottom view); (c) connected diversity rectenna (top view).

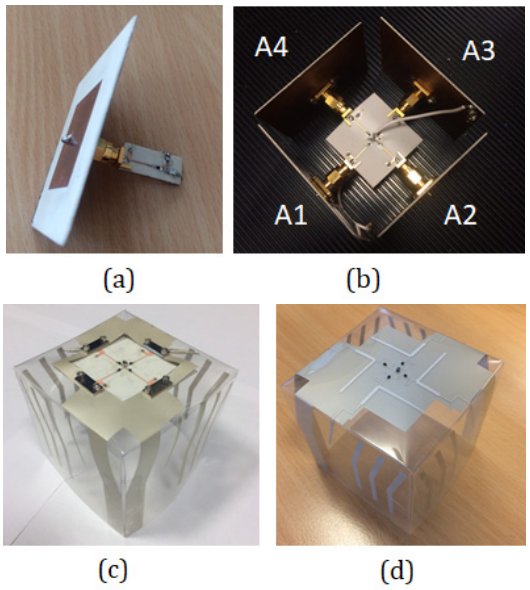

FIGURE 17. Photo of fabricated Rectenna (a) Rectenna 1A (Scenario S2); (b) Rectifier 1B (Scenario S3); (c) Rectenna 2 (Scenario S4); (d) Rectenna 3 (Scenario S5).

the performance of diversity antenna system operating in an indoor environment.

The scenario S4 and scenario S5 used the proposed flexible antenna diversity with separated rectifier (Rectenna 2 - Fig.17c) and integrated rectifier (Rectenna 3 - Fig.17d), respectively. The integration between separated rectifier and the antennas is presented in Fig. 13. These scenarios compare the performance of the proposed flexible rectenna diversity and conventional patch diversity.

Fig.18 describes the measurement setup of the tests using two transmitting antennas in a realistic environment with office facilities around. Two identical commercial antennas for a Wi-Fi router with a gain of 5 dB were used as transmission antennas. Transmission source A was set at 15 dBm, hence the equivalent isotropic radiated power (EIRP) is 100 mW, corresponding to the maximum transmission power of a conventional Wi-Fi router. The transmission source B was set at 12 dBm, which is equivalent to an EIRP of 50 mW. The elevation of two transmission antennas was fixed at 1.5 m and the elevation of the reception antennas was fixed at 0.8 m.

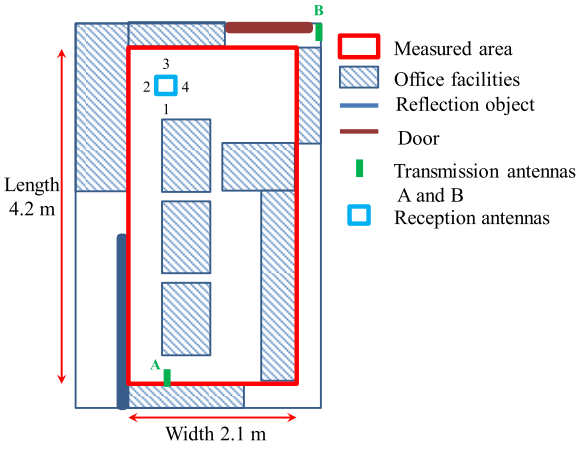

FIGURE 18. Measurement setup.

V. MEASUREMENT RESULTS

A. ANTENNA MEASUREMENT

The prototype of the flat structure of the proposed diversity design was fabricated by screen printing technology on the PET substrate with a silver conductive ink Electrodag PF-410 and the impression was performed using manual screen printer Svecia Semimatic SSM.

The 3D rectenna in the form of system packaging was formed by folding the flat structure at four edges. There are two ways to fold the proposed circuit, where the rectifier circuit can be inside or outside the cube depending on the application needs. The end-launch connectors were also used to perform the S-parameters at each port of the diversity antenna.

The four flexible antennas have been characterized using a VNA Anritsu 37369A. The 3D flexible diversity antenna in Fig. 19 was connected to end-launch connectors while keeping the rectifier ground plane to ensure the operating conditions of the system as described in section III.B. The rectifier part was cut out of the circuit, then stucked in place by tape (Fig. 19). This configuration is implemented in order to measure the performance of the antenna's part only, without connecting with rectifier's part but still taking into account any ground effect.

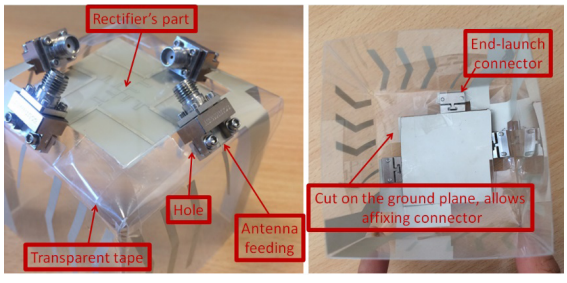

FIGURE 19. Photo of 3D diversity antenna with end-launch connectors.

Fig. 20 presents the comparison between simulation and experimental reflection coefficients at four ports. The results

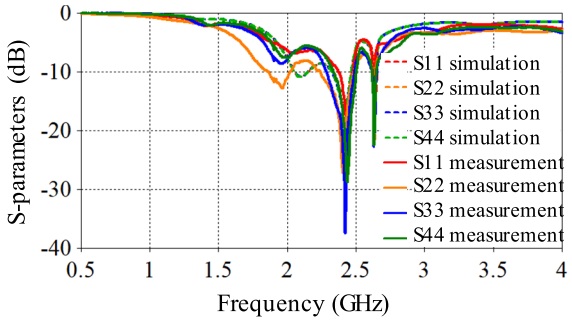

FIGURE 20. Simulation and measurement of reflection coefficient of four antennas in the diversity antenna system.

show the good matching for four antennas at the resonant frequency of 2.45 GHz. The -10 dB impedance bandwidths of four antennas, which cover the band of WLAN 2.4 GHz, are provided in Table 2.

TABLE 2. Measured bandwidth of four antennas at 2.4 GHz.

Bandwidth	Antenna 1	Antenna 2	Antenna 3	Antenna 4
Frequency (GHz)	2.35 – 2.48	2.24-2.48	2.28-2.49	2.33-2.51
MHz	130	240	210	180
%	5.4	10	8.7	7.5

The isolation between ports is presented in Fig. 21. Table 3 shows the comparison of results for S-parameters between simulation and measurement for the diversity antenna at frequency 2.45 GHz. It can be seen that results agreement between simulation and measurement is satisfying for both impedance matching and the isolation between ports. The coupling between the most sensible pair ANT1 and ANT2, followed by ANT3 and ANT4 respectively, has been eliminated by the proposed technique.

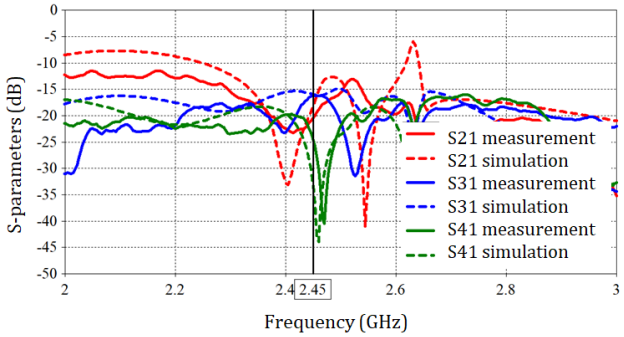

FIGURE 21. Mutual coupling between antenna ANT1 and others antennas (dB).

The measurement of radiation pattern was performed in an anechoic chamber and the E-plane measurement of each antenna at $\varphi = 0$ is shown in Fig. 22. The maximum measured gain in each direction is 5.96 dBi, which is quite close to the simulated result. The beam axis of each antenna is not orthogonal as desired to cover equally the space. This

TABLE 3. Comparison of S-parameters between simulation and measurement at 2.45 GHz.

Reflection coefficient (dB)	S11	S22	S33	S44
Simulation	-12.9	-12.9	-12.6	-12.8
Measurement	-20.2	-14.0	-17.3	-23.9
Isolation (dB)		S21	S31	S41
Simulation		-18.2	-16	-33.3
Measurement		-20.4	-16.2	-24.6

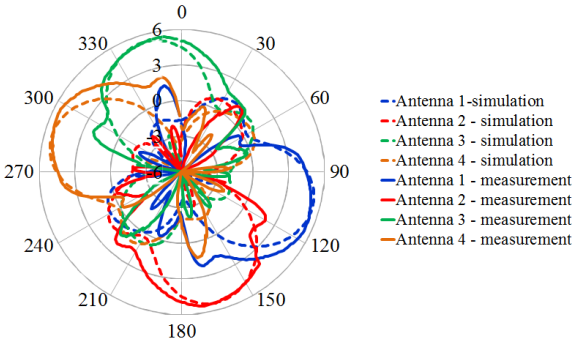

FIGURE 22. Simulation and measurement of E-plane radiation pattern of four antennas.

observation can be explained by the pair-based symmetric design in the placement of antennas. The axis where the radiation pattern did not reach a maximum is the position covered by the reflectors of the antennas.

B. RECTIFIER MEASUREMENT

The single-input rectifier A and four-input rectifier B were fabricated on RO 4003 substrate. The generator Agilent PSG E8257D was used to generate the RF source for the measurement of the rectifiers. The rectifier B can work in balanced state (with four active inputs of the same level) or unbalanced state (with only one active input or one dominant input).

Fig.23 presents the harvested power in three cases: rectifier A, rectifier B (only one active input) and rectifier B (four active inputs), with input power from −45 to −20 dBm.

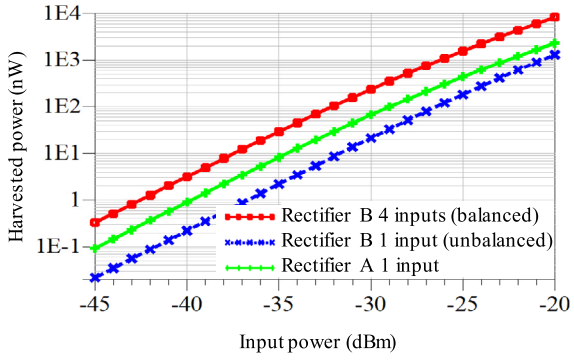

FIGURE 23. Measured output power versus input power of rectifier A and rectifier B in case of balanced and unbalanced input.

The harvested power of rectifier A is 12.8 nW at -34 dBm, equivalent to a RF-DC conversion efficiency of 3.21%. The harvested power of rectifier B (unbalanced state) is 3.5 nW and rectifier B (balanced state) produced 45.1 nW. The RF-DC conversion efficiency of rectifier B is 2.6% at −34 dBm while having four balanced inputs. The latter results support the simulation observations.

However, the actual effect of the rectifier B can only be assessed through measurement in realistic scenario, when combined with antennas.

C. RECTENNA MEASUREMENT IN REALISTIC ENVIRONMENT

The scenario S1 was conducted in order to estimate the available power in ambiance at each point and direction. For 80% of the measurement points, power level differences (*DeltaP*) in each direction were less than 10 dB. Kernel density estimation method was used to estimate the probability density function (PDF) and cumulative density function (CDF) of measured power. The CDF assessed at each value of received power is the probability that the received power less than or equal to that value. The median harvested power is the 50th percentile of the probability distribution and this value is calculated with the help of Matlab's median function and observed in a graph of CDF, which corresponds to the value of 0.5 on the vertical axis.

The PDF and CDF of available power measurement results in scenario S1 are presented in Fig.24. Its median value is −34 dBm, which is equivalent to a median density power of 10.8 nW/cm2 or 0.1 mW/m2.

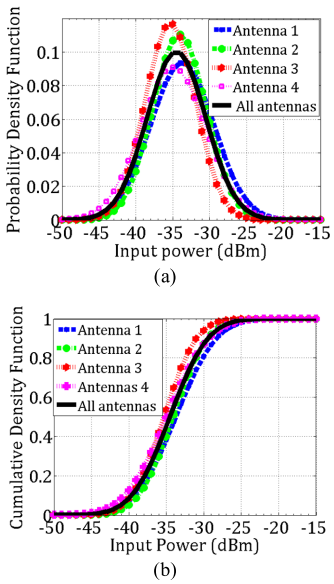

FIGURE 24. (a) Probability density function (PDF); (b) Cumulative density function (CDF) of measured input power (dBm) across different directions of antenna in scenario S1.

The harvested power distributions of single rectennas are presented in Fig.25a, b, c, d in each direction of antenna (as described in Fig.18) respectively when conducting scenario

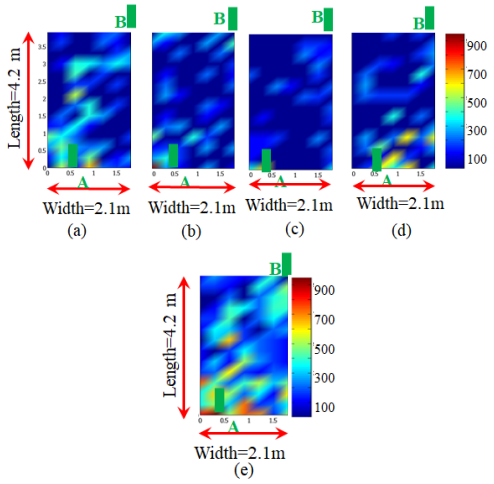

FIGURE 25. Scenario S2: haversted power distribution (nW) in space for each rectenna with (a) Antenna 1; (b) Antenna 2; (c) Antenna 3; (d) Antenna 4; (e) Scenario S3: All four antennas (as described in Fig.18).

S2. The results show a different pattern of each direction in the multipath environment and it shows the wasted harvestable energy in space while using only one antenna with a limited beam solid angle. The received power is unevenly distributed in each direction.

Fig.25e shows the harvested power distribution in space from multi-angle diversity rectenna (Rectenna 1B).

When there is only one input, rectifier B has a lower efficiency in comparison with rectifier A because of the loss in the three other branches (Fig.23). That explains the result where in 30 points over 98 points of measurement, harvested power of rectenna 1B is lower than the one from rectenna 1A. Nonetheless, the level and density of harvested power from diversity structure is higher in general.

The PDF and the CDF of harvested power among scenarios S2, S3, S4, S5 are described in Fig.26 and Fig. 27 respectively. This empirical graph was then compared with other analytical distributions such as Rayleigh, Weibull, Ricean, Nakagami and Log-Normal using the same group of data. The results show that in this configuration of measurement, inside the working office, the received power has the Log-Normal distributions. While the measurement setup consisted of

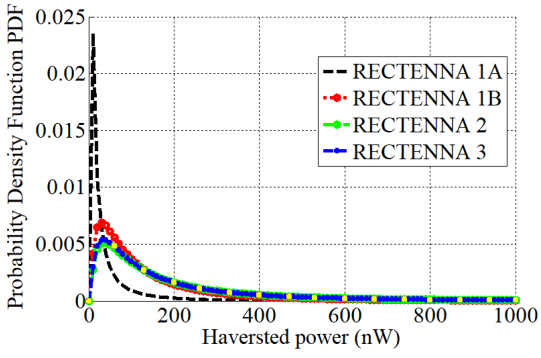

FIGURE 26. PDF of harvested power (nW) from four rectennas and four scenarios.

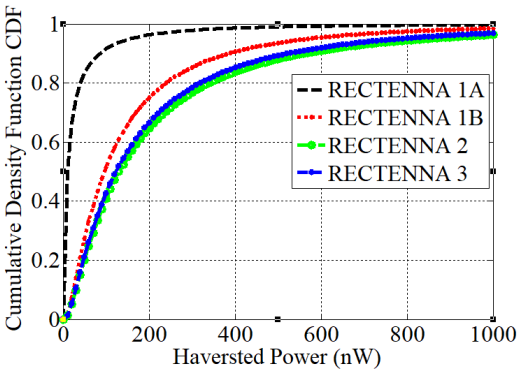

FIGURE 27. CDF of harvested power (nW) from four rectennas and four scenarios.

TABLE 4. Comparison of harvested power (HP) between configurations.

Rectenna	Probability HP higher than 200 nW at 0.1 mW/m^2 ambience	Median HP (nW)	Median RF-DC efficiency at 0.1 mW/m^2 ambience
Rectenna 1A	4%	10	2.5%
Rectenna 1B	25%	97	6.1%
Rectenna 2	36%	130	6.4%
Rectenna 3	33%	124	6.1%

many reflective objects, this finding approves the typical feature of Log-Normal distribution as described in theory.

The results support that by using the proposed flexible antenna (rectenna 2 and 3), the probability of receiving higher power increases because the proposed antennas have higher gain compared to the conventional patch antenna. However, rectenna 3 with integrated circuit has lower performance than rectenna 2 due to the loss in the PET substrate of the rectifier. The comparison of performance between configurations is provided in Table 4.

The median harvested power of the proposed 3D flexible structure is 124 nW, which corresponds to a nominal RF-DC conversion efficiency of 6.1% at a median input power of 0.1mW/m2. Results strongly support that by using a diversity antenna system, the likelihood of receiving power greatly increases. The probability that the harvested power becomes better than 200 nW is 4% when using rectenna 1A, 25% when using rectenna 1B, 36% when using rectenna 2 and 33% when using rectenna 3. The median harvested power increases to 130 nW when using rectenna 2 and 124 nW by using rectenna 3. Though rectenna 3 performs slightly lower compared to the separated one, the ease of fabrication, simplicity and the lightweight are still strong advantages of the proposed 3D flexible diversity rectenna.

VI. CONCLUSION

This paper has presented a study about 3D flexible diversity antenna, which takes advantage of the packaging form for ambient RF energy scavenging operation in an indoor environment. Results illustrate the benefits of diversity antenna systems, especially at a low power density environment, about 0.1 mW/m2. Observations strongly suggest that by using this technique, the fading of received signals across random points in space is mitigated.

In addition, to overcome the drawbacks of the flexible substrate itself, a technique to decrease mutual coupling was also proposed. The mutual coupling between antennas decreases significantly with minor adjustment, while the gain in each direction reaches about 5.96 dBi. The flexible rectenna in diversity design increases the probability of harvested power higher than 200 nW from 4% for one conventional patch to 33% for a full system. Additionally, the probability of higher harvested power value was drastically increased. The median harvested power is 12 times higher than using a singular antenna. The system efficiency is also higher in comparison to a single structure.

The results have shown the effectiveness of the proposed system in terms of received power and practicality of its form as a system packaging. While the design of auxiliary circuitry is better on conventional substrate, the advantages gained through the usage of flexible material for IoT antenna systems are very promising. In the future perspective, further development of polarization diversity is expected, by a trade-off with the gain of antenna in one direction. Additional measurement setup will also be arranged to cover different scenarios of indoor environment.

ACKNOWLEDGMENT

The authors would like to thank Arjowiggins Creative Papers for their support in the fabrication circuit during this work.

REFERENCES

[1] U. Olgun, C.-C. Chen, and J. L. Volakis, "Design of an efficient ambient WiFi energy harvesting system," *IET Microw., Antennas Propag.*, vol. 6, no. 11, pp. 1200–1206, Aug. 2012.

[2] J. Kimionis, M. Isakov, B. S. Koh, A. Georgiadis, and M. M. Tentzeris, "3D-printed origami packaging with inkjet-printed antennas for RF harvesting sensors," *IEEE Trans. Microw. Theory Techn.*, vol. 63, no. 12, pp. 4521–4532, Dec. 2015.

[3] C. Song *et al.*, "A novel six-band dual CP rectenna using improved impedance matching technique for ambient RF energy harvesting," *IEEE Trans. Antennas Propag.*, vol. 64, no. 7, pp. 3160–3171, Jul. 2016.

[4] M. Pinuela, P. D. Mitcheson, and S. Lucyszyn, "Ambient RF energy harvesting in urban and semi-urban environments," *IEEE Trans. Microw. Theory Techn.*, vol. 61, no. 7, pp. 2715–2726, Jul. 2013.

[5] L. Yang, Y. J. Zhou, C. Zhang, X. M. Yang, X.-X. Yang, and C. Tan, "Compact multiband wireless energy harvesting based battery-free body area networks sensor for mobile healthcare," *IEEE J. Electromagn., RF Microw. Med. Biol.*, vol. 2, no. 2, pp. 109–115, Jun. 2018.

[6] C. M. Kruesi, R. J. Vyas, and M. M. Tentzeris, "Design and development of a novel 3-D cubic antenna for wireless sensor networks (WSNs) and RFID applications," *IEEE Trans. Antennas Propag.*, vol. 57, no. 10, pp. 3293–3299, Oct. 2009.

[7] X. Zhang, H. Liu, and L. Li, "Tri-band miniaturized wide-angle and polarization-insensitive metasurface for ambient energy harvesting," *Appl. Phys. Lett.*, vol. 111, no. 7, 2017, Art. no. 071902.

[8] H. Zhong, X.-X. Yang, C. Tan, and K. Yu, "Triple-band polarization-insensitive and wide-angle metamaterial array for electromagnetic energy harvesting," *Appl. Phys. Lett.*, vol. 109, no. 25, pp. 1–5, 2016.

[9] T. Q. Van Hoang, L. H. Trinh, F. Ferrero, E. Séguenot, T.-P. Vuong, and J.-L. Dubard, "Rectenna measurement in a realistic environment," in *Proc. IEEE Conf. Antenna Meas. Appl. (CAMA)*, Nov. 2014, pp. 1–4.

[10] E. Vandelle *et al.*, "High gain isotropic rectenna," in *Proc. IEEE Wireless Power Transf. Conf. (WPTC)*, May 2017, pp. 1–4.

[11] F. Fezai, C. Menudier, M. Thevenot, T. Monediere, and N. Chevalier, "Multidirectional receiving system for RF to dc conversion signal: Application to home automation devices." *IEEE Antennas Propag. Mag.*, vol. 58, no. 3, pp. 22–30, Jun. 2016.
[12] D. H. N. Bui, *Printed Flexible Antenna for Energy Harvesting*, Optics and Photonic. Université Grenoble Alpes, Saint-Martin-d'Hères, France, 2017.
[13] T. K. Sarkar, Z. Ji, K. Kim, A. Medouri, and M. Salazar-Palma, "A survey of various propagation models for mobile communication," *IEEE Antennas Propag. Mag.*, vol. 45, no. 3, pp. 51–82, Jun. 2003.
[14] T. S. Rappaport, *Wireless Communications: Principles and Practice*. Upper Saddle River, NJ, USA: Prentice-Hall, 2002, p. 680.
[15] M. Y. Naderi, K. R. Chowdhury, and S. Basagni, "Wireless sensor networks with RF energy harvesting: Energy models and analysis," in *Proc. IEEE Wireless Commun. Netw. Conf. (WCNC)*, Mar. 2015, pp. 1494–1499.
[16] A. U. Sheikh, M. Abdi, and M. Handforth, "Indoor mobile radio channel at 946 MHz: Measurements and modeling," in *Proc. IEEE 43rd Veh. Technol. Conf.*, May 1993, pp. 73–76.
[17] C. A. Balanis, *Antenna Theory: Analysis and Design*, 3rd ed. Hoboken, NJ, USA: Wiley, 2012.
[18] T. Q. V. Hoang, E. Seguenot, F. Ferrero, J. Dubard, P. Brachat, and J. Desvilles, "3D Voltage pattern measurement of a 2.45 GHz rectenna," *IEEE Trans. Antennas Propag.*, vol. 61, no. 6, pp. 3354–3356, Jun. 2013.
[19] Y. Chung, S.-S. Jeon, D. Ahn, J.-I. Choi, and T. Itoh, "High isolation dual-polarized patch antenna using integrated defected ground structure," *IEEE Microw. Wireless Compon. Lett.*, vol. 14, no. 1, pp. 4–6, Jan. 2004.
[20] C.-M. Luo, J.-S. Hong, and L.-L. Zhong, "Isolation enhancement of a very compact UWB-MIMO slot antenna with two defected ground structures," *IEEE Antennas Wireless Propag. Lett.*, vol. 14, pp. 1766–1769, 2015.
[21] H. Li, "Decoupling and evaluation of multiple antenna systems in compact MIMO terminals," Ph.D. dissertation, Elect. Eng., KTH Royal Inst. Technol., Stockholm, Sweden, 2012.
[22] V. Marian, C. Menudier, M. Thevenot, C. Vollaire, J. Verdier, and B. Allard, "Efficient design of rectifying antennas for low power detection," in *IEEE MTT-S Int. Microw. Symp. Dig.*, Jun. 2011, pp. 1–4.

DO HANH NGAN BUI (M'14) received the M.Sc. degree in microwaves from the Grenoble Institute of Technology, Grenoble, France, in 2009, and the Ph.D. degree in radiofrequency from the University of Grenoble Alpes, Grenoble, in 2017. Since 2017, she has been a Researcher with the IMEP–LAHC Laboratory, Grenoble. Her research interests include the domain of energy harvesting and printed electronics.

TAN-PHU VUONG (SM'08) received the Ph.D. degree in microwave engineering from INP Toulouse, France, in 1999. From 2001 to 2008, he was an Associate Professor of microwave engineering with the School of Advanced Systems and Networks. Since 2008, he has been a Professor with the School of Engineering in Physics, Applied Physics, Electronics and Materials Science (Phelma), Grenoble INP. He has authored or co-authored more than 180 referred papers and two book chapters, and holds three patents. His current research interests involve substrate integrated circuits, small antennas, printed antennas, antenna arrays, advanced computer-aided design and modeling techniques, wireless power transmission and harvesting, and the development of low-cost RF, electronic printed shielding, RF identification, and sensors for wireless systems, security techniques, and biomedical applications.

JACQUES VERDIER was born in Toulouse, France, in 1969. He received the M.S. degree in electrical engineering from the University of Toulouse, Toulouse, in 1997. Since 1998, he has been an Associate Professor with the Institut National des Sciences Appliquées de Lyon, Villeurbanne, France. In 1998, he joined the Institut des Nanotechnologies de Lyon (UMR-CNRS 5270). He is involved in research on agile radio resource sharing (hardware architecture of systems), in particular on the topic of energy harvesting and wireless energy transfer. His research interests include the modeling and characterization of noise in nonlinear microwave circuits and analog and RF IC design for wireless communications in BiCMOS and CMOS technologies.

BRUNO ALLARD (M'93–SM'02) received the M.Sc. and Ph.D. degrees in engineering from INSA Lyon, France, in 1989 and 1992, respectively. He is currently a Full Professor in electrical engineering with the Institut National des Sciences Appliquées de Lyon, Lyon. He is also the Director of the Laboratory Ampère. He has led numerous industrial and academic projects. He has authored or co-authored more than 120 papers in Transactions and journals and 300 international conference contributions. His research interests include the integration of power systems, either hybrid or monolithic, power semiconductor device modeling and characterization, power electronic system design, and low-power monolithic converter design.

PHILIPPE BENECH (M'08) received the M.S. degree in microelectronics from the University of Montpellier, in 1987, and the Ph.D. degree in instrumentation from University Grenoble, France, in 1990. Since 2000, he has been a Professor with the University of Grenoble Alpes. His research interests include the domain of radio frequency components, devices, and integrated functions.